

Measurements of Absolute Branching Fractions for $\Lambda_c^+ \rightarrow \Xi^0 K^+$ and $\Xi(1530)^0 K^+$

M. Ablikim¹, M. N. Achasov^{9,d}, S. Ahmed¹⁴, M. Albrecht⁴, M. Alekseev^{55A,55C}, A. Amoroso^{55A,55C}, F. F. An¹, Q. An^{52,42}, J. Z. Bai¹, Y. Bai⁴¹, O. Bakina²⁶, R. Baldini Ferroli^{22A}, Y. Ban³⁴, D. W. Bennett²¹, J. V. Bennett⁵, N. Berger²⁵, M. Bertani^{22A}, D. Bettoni^{23A}, F. Bianchi^{55A,55C}, E. Boger^{26,b}, I. Boyko²⁶, R. A. Briere⁵, H. Cai⁵⁷, X. Cai^{1,42}, O. Cakir^{45A}, A. Calcaterra^{22A}, G. F. Cao^{1,46}, S. A. Cetin^{45B}, J. Chai^{55C}, J. F. Chang^{1,42}, G. Chelkov^{26,b,c}, G. Chen¹, H. S. Chen^{1,46}, J. C. Chen¹, M. L. Chen^{1,42}, P. L. Chen⁵³, S. J. Chen³², X. R. Chen²⁹, Y. B. Chen^{1,42}, X. K. Chu³⁴, G. Cibinetto^{23A}, F. Cossio^{55C}, H. L. Dai^{1,42}, J. P. Dai^{37,h}, A. Dbeysy¹⁴, D. Dedovich²⁶, Z. Y. Deng¹, A. Denig²⁵, I. Denysenko²⁶, M. Destefanis^{55A,55C}, F. De Mori^{55A,55C}, Y. Ding³⁰, C. Dong³³, J. Dong^{1,42}, L. Y. Dong^{1,46}, M. Y. Dong^{1,42,46}, Z. L. Dou³², S. X. Du⁶⁰, P. F. Duan¹, J. Fang^{1,42}, S. S. Fang^{1,46}, Y. Fang¹, R. Farinelli^{23A,23B}, L. Fava^{55B,55C}, S. Fegan²⁵, F. Feldbauer⁴, G. Felici^{22A}, C. Q. Feng^{52,42}, E. Fioravanti^{23A}, M. Fritsch⁴, C. D. Fu¹, Q. Gao¹, X. L. Gao^{52,42}, Y. Gao⁴⁴, Y. G. Gao⁶, Z. Gao^{52,42}, B. Garillon²⁵, I. Garzia^{23A}, K. Goetzen¹⁰, L. Gong³³, W. X. Gong^{1,42}, W. Gradl²⁵, M. Greco^{55A,55C}, M. H. Gu^{1,42}, Y. T. Gu¹², A. Q. Guo¹, R. P. Guo^{1,46}, Y. P. Guo²⁵, Z. Haddadi²⁸, S. Han⁵⁷, X. Q. Hao¹⁵, F. A. Harris⁴⁷, K. L. He^{1,46}, X. Q. He⁵¹, F. H. Heinsius⁴, T. Held⁴, Y. K. Heng^{1,42,46}, T. Holtmann⁴, Z. L. Hou¹, H. M. Hu^{1,46}, J. F. Hu^{37,h}, T. Hu^{1,42,46}, Y. Hu¹, G. S. Huang^{52,42}, J. S. Huang¹⁵, X. T. Huang³⁶, X. Z. Huang³², Z. L. Huang³⁰, T. Hussain⁵⁴, W. Ikegami Andersson⁵⁶, Q. Ji¹, Q. P. Ji¹⁵, X. B. Ji^{1,46}, X. L. Ji^{1,42}, X. S. Jiang^{1,42,46}, X. Y. Jiang³³, J. B. Jiao³⁶, Z. Jiao¹⁷, D. P. Jin^{1,42,46}, S. Jin^{1,46}, Y. Jin⁴⁸, T. Johansson⁵⁶, A. Julin⁴⁹, N. Kalantar-Nayestanaki²⁸, X. S. Kang³³, M. Kavatsyuk²⁸, B. C. Ke⁵, T. Khan^{52,42}, A. Khoukaz⁵⁰, P. Kiese²⁵, R. Kliemt¹⁰, L. Koch²⁷, O. B. Kolcu^{45B,f}, B. Kopf⁴, M. Kornicer⁴⁷, M. Kuemmel⁴, M. Kuessner⁴, M. Kuhlmann⁴, A. Kupsc⁵⁶, W. Kühn²⁷, J. S. Lange²⁷, M. Lara²¹, P. Larin¹⁴, L. Lavezzi^{55C}, H. Leithoff²⁵, C. Leng^{55C}, C. Li⁵⁶, Cheng Li^{52,42}, D. M. Li⁶⁰, F. Li^{1,42}, F. Y. Li³⁴, G. Li¹, H. B. Li^{1,46}, H. J. Li^{1,46}, J. C. Li¹, Jin Li³⁵, K. J. Li⁴³, Kang Li¹³, Ke Li¹, Lei Li³, P. L. Li^{52,42}, P. R. Li^{29,46,7}, Q. Y. Li³⁶, W. D. Li^{1,46}, W. G. Li¹, X. L. Li³⁶, X. N. Li^{1,42}, X. Q. Li³³, Z. B. Li⁴³, H. Liang^{52,42}, Y. F. Liang³⁹, Y. T. Liang²⁷, G. R. Liao¹¹, J. Libby²⁰, D. X. Lin¹⁴, B. Liu^{37,h}, B. J. Liu¹, C. X. Liu¹, D. Liu^{52,42}, F. H. Liu³⁸, Fang Liu¹, Feng Liu⁶, H. B. Liu¹², H. M. Liu^{1,46}, Huanhuan Liu¹, Huihui Liu¹⁶, J. B. Liu^{52,42}, J. Y. Liu^{1,46}, K. Liu⁴⁴, K. Y. Liu³⁰, Ke Liu⁶, L. D. Liu³⁴, Q. Liu⁴⁶, S. B. Liu^{52,42}, X. Liu²⁹, Y. B. Liu³³, Z. A. Liu^{1,42,46}, Zhiqing Liu²⁵, Y. F. Long³⁴, X. C. Lou^{1,42,46}, H. J. Lu¹⁷, J. G. Lu^{1,42}, Y. Lu¹, Y. P. Lu^{1,42}, C. L. Luo³¹, M. X. Luo⁵⁹, X. L. Luo^{1,42}, S. Lusso^{55C}, X. R. Lyu⁴⁶, F. C. Ma³⁰, H. L. Ma¹, L. L. Ma³⁶, M. M. Ma^{1,46}, Q. M. Ma¹, T. Ma¹, X. N. Ma³³, X. Y. Ma^{1,42}, Y. M. Ma³⁶, F. E. Maas¹⁴, M. Maggiora^{55A,55C}, Q. A. Malik⁵⁴, Y. J. Mao³⁴, Z. P. Mao¹, S. Marcelllo^{55A,55C}, Z. X. Meng⁴⁸, J. G. Messchendorp²⁸, G. Mezzadri^{23B}, J. Min^{1,42}, R. E. Mitchell²¹, X. H. Mo^{1,42,46}, Y. J. Mo⁶, C. Morales Morales¹⁴, N. Yu. Muchnoi^{9,d}, H. Muramatsu⁴⁹, A. Mustafa⁴, Y. Nefedov²⁶, F. Nerling¹⁰, I. B. Nikolaev^{9,d}, Z. Ning^{1,42}, S. Nisar⁸, S. L. Niu^{1,42}, X. Y. Niu^{1,46}, S. L. Olsen^{35,j}, Q. Ouyang^{1,42,46}, S. Pacetti^{22B}, Y. Pan^{52,42}, M. Papenbrock⁵⁶, P. Patteri^{22A}, M. Pelizaeus⁴, J. Pellegrino^{55A,55C}, H. P. Peng^{52,42}, K. Peters^{10,g}, J. Pettersson⁵⁶, J. L. Ping³¹, R. G. Ping^{1,46}, A. Pitka⁴, R. Poling⁴⁹, V. Prasad^{52,42}, H. R. Qi², M. Qi³², T. Y. Qi², S. Qian^{1,42}, C. F. Qiao⁴⁶, N. Qin⁵⁷, X. S. Qin⁴, Z. H. Qin^{1,42}, J. F. Qiu¹, K. H. Rashid^{54,i}, C. F. Redmer²⁵, M. Richter⁴, M. Ripka²⁵, M. Rolo^{55C}, G. Rong^{1,46}, Ch. Rosner¹⁴, A. Sarantsev^{26,e}, M. Savrić^{23B}, C. Schnier⁴, K. Schoenning⁵⁶, W. Shan¹⁸, X. Y. Shan^{52,42}, M. Shao^{52,42}, C. P. Shen², P. X. Shen³³, X. Y. Shen^{1,46}, H. Y. Sheng¹, X. Shi^{1,42}, J. J. Song³⁶, W. M. Song³⁶, X. Y. Song¹, S. Sosio^{55A,55C}, C. Sowa⁴, S. Spataro^{55A,55C}, G. X. Sun¹, J. F. Sun¹⁵, L. Sun⁵⁷, S. S. Sun^{1,46}, X. H. Sun¹, Y. J. Sun^{52,42}, Y. K. Sun^{52,42}, Y. Z. Sun¹, Z. J. Sun^{1,42}, Z. T. Sun²¹, Y. T. Tan^{52,42}, C. J. Tang³⁹, G. Y. Tang¹, X. Tang¹, I. Tapan^{45C}, M. Tiemens²⁸, B. Tsednee²⁴, I. Uman^{45D}, G. S. Varner⁴⁷, B. Wang¹, B. L. Wang⁴⁶, D. Wang³⁴, D. Y. Wang³⁴, Dan Wang⁴⁶, K. Wang^{1,42}, L. L. Wang¹, L. S. Wang¹, M. Wang³⁶, Meng Wang^{1,46}, P. Wang¹, P. L. Wang¹, W. P. Wang^{52,42}, X. F. Wang⁴⁴, Y. D. Wang¹⁴, Y. F. Wang^{1,42,46}, Y. Q. Wang²⁵, Z. Wang^{1,42}, Z. G. Wang^{1,42}, Z. Y. Wang¹, Zongyuan Wang^{1,46}, T. Weber⁴, D. H. Wei¹¹, P. Weidenkaff²⁵, S. P. Wen¹, U. Wiedner⁴, M. Wolke⁵⁶, L. H. Wu¹, L. J. Wu^{1,46}, Z. Wu^{1,42}, L. Xia^{52,42}, Y. Xia¹⁹, D. Xiao¹, Y. J. Xiao^{1,46}, Z. J. Xiao³¹, Y. G. Xie^{1,42}, Y. H. Xie⁶, X. A. Xiong^{1,46}, Q. L. Xiu^{1,42}, G. F. Xu¹, J. J. Xu^{1,46}, L. Xu¹, Q. J. Xu¹³, Q. N. Xu⁴⁶, X. P. Xu⁴⁰, L. Yan^{55A,55C}, W. B. Yan^{52,42}, W. C. Yan², Y. H. Yan¹⁹, H. J. Yang^{37,h}, H. X. Yang¹, L. Yang⁵⁷, Y. H. Yang³², Y. X. Yang¹¹, M. Ye^{1,42}, M. H. Ye⁷, J. H. Yin¹, Z. Y. You⁴³, B. X. Yu^{1,42,46}, C. X. Yu³³, J. S. Yu²⁹, C. Z. Yuan^{1,46}, Y. Yuan¹, A. Yuncu^{45B,a}, A. A. Zafar⁵⁴, Y. Zeng¹⁹, Z. Zeng^{52,42}, B. X. Zhang¹, B. Y. Zhang^{1,42}, C. C. Zhang¹, D. H. Zhang¹, H. H. Zhang⁴³, H. Y. Zhang^{1,42}, J. Zhang^{1,46}, J. L. Zhang⁵⁸, J. Q. Zhang⁴, J. W. Zhang^{1,42,46}, J. Y. Zhang¹, J. Z. Zhang^{1,46}, K. Zhang^{1,46}, L. Zhang⁴⁴, X. Y. Zhang³⁶, Y. Zhang^{52,42}, Y. H. Zhang^{1,42}, Y. T. Zhang^{52,42}, Yang Zhang¹, Yao Zhang¹, Yu Zhang⁴⁶, Z. H. Zhang⁶, Z. P. Zhang⁵², Z. Y. Zhang⁵⁷, G. Zhao¹, J. W. Zhao^{1,42}, J. Y. Zhao^{1,46}, J. Z. Zhao^{1,42}, Lei Zhao^{52,42}, Ling Zhao¹, M. G. Zhao³³, Q. Zhao¹, S. J. Zhao⁶⁰, T. C. Zhao¹, Y. B. Zhao^{1,42}, Z. G. Zhao^{52,42}, A. Zhemchugov^{26,b}, B. Zheng⁵³, J. P. Zheng^{1,42}, W. J. Zheng³⁶, Y. H. Zheng⁴⁶, B. Zhong³¹, L. Zhou^{1,42}, X. Zhou⁵⁷, X. K. Zhou^{52,42}, X. R. Zhou^{52,42}, X. Y. Zhou¹, J. Zhu³³, J. Zhu⁴³, K. Zhu¹, K. J. Zhu^{1,42,46}, S. Zhu¹, S. H. Zhu⁵¹, X. L. Zhu⁴⁴, Y. C. Zhu^{52,42}, Y. S. Zhu^{1,46}, Z. A. Zhu^{1,46}, J. Zhuang^{1,42}, B. S. Zou¹, J. H. Zou¹

(BESIII Collaboration)

- ¹ Institute of High Energy Physics, Beijing 100049, People's Republic of China
- ² Beihang University, Beijing 100191, People's Republic of China
- ³ Beijing Institute of Petrochemical Technology, Beijing 102617, People's Republic of China
- ⁴ Bochum Ruhr-University, D-44780 Bochum, Germany
- ⁵ Carnegie Mellon University, Pittsburgh, Pennsylvania 15213, USA
- ⁶ Central China Normal University, Wuhan 430079, People's Republic of China
- ⁷ China Center of Advanced Science and Technology, Beijing 100190, People's Republic of China
- ⁸ COMSATS Institute of Information Technology, Lahore, Defence Road, Off Raiwind Road, 54000 Lahore, Pakistan
- ⁹ G.I. Budker Institute of Nuclear Physics SB RAS (BINP), Novosibirsk 630090, Russia
- ¹⁰ GSI Helmholtzcentre for Heavy Ion Research GmbH, D-64291 Darmstadt, Germany
- ¹¹ Guangxi Normal University, Guilin 541004, People's Republic of China
- ¹² Guangxi University, Nanning 530004, People's Republic of China
- ¹³ Hangzhou Normal University, Hangzhou 310036, People's Republic of China
- ¹⁴ Helmholtz Institute Mainz, Johann-Joachim-Becher-Weg 45, D-55099 Mainz, Germany
- ¹⁵ Henan Normal University, Xinxiang 453007, People's Republic of China
- ¹⁶ Henan University of Science and Technology, Luoyang 471003, People's Republic of China
- ¹⁷ Huangshan College, Huangshan 245000, People's Republic of China
- ¹⁸ Hunan Normal University, Changsha 410081, People's Republic of China
- ¹⁹ Hunan University, Changsha 410082, People's Republic of China
- ²⁰ Indian Institute of Technology Madras, Chennai 600036, India
- ²¹ Indiana University, Bloomington, Indiana 47405, USA
- ²² (A)INFN Laboratori Nazionali di Frascati, I-00044, Frascati, Italy; (B)INFN and University of Perugia, I-06100, Perugia, Italy
- ²³ (A)INFN Sezione di Ferrara, I-44122, Ferrara, Italy; (B)University of Ferrara, I-44122, Ferrara, Italy
- ²⁴ Institute of Physics and Technology, Peace Ave. 54B, Ulaanbaatar 13330, Mongolia
- ²⁵ Johannes Gutenberg University of Mainz, Johann-Joachim-Becher-Weg 45, D-55099 Mainz, Germany
- ²⁶ Joint Institute for Nuclear Research, 141980 Dubna, Moscow region, Russia
- ²⁷ Justus-Liebig-Universitaet Giessen, II. Physikalisches Institut, Heinrich-Buff-Ring 16, D-35392 Giessen, Germany
- ²⁸ KVI-CART, University of Groningen, NL-9747 AA Groningen, The Netherlands
- ²⁹ Lanzhou University, Lanzhou 730000, People's Republic of China
- ³⁰ Liaoning University, Shenyang 110036, People's Republic of China
- ³¹ Nanjing Normal University, Nanjing 210023, People's Republic of China
- ³² Nanjing University, Nanjing 210093, People's Republic of China
- ³³ Nankai University, Tianjin 300071, People's Republic of China
- ³⁴ Peking University, Beijing 100871, People's Republic of China
- ³⁵ Seoul National University, Seoul, 151-747 Korea
- ³⁶ Shandong University, Jinan 250100, People's Republic of China
- ³⁷ Shanghai Jiao Tong University, Shanghai 200240, People's Republic of China
- ³⁸ Shanxi University, Taiyuan 030006, People's Republic of China
- ³⁹ Sichuan University, Chengdu 610064, People's Republic of China
- ⁴⁰ Soochow University, Suzhou 215006, People's Republic of China
- ⁴¹ Southeast University, Nanjing 211100, People's Republic of China
- ⁴² State Key Laboratory of Particle Detection and Electronics, Beijing 100049, Hefei 230026, People's Republic of China
- ⁴³ Sun Yat-Sen University, Guangzhou 510275, People's Republic of China
- ⁴⁴ Tsinghua University, Beijing 100084, People's Republic of China
- ⁴⁵ (A)Ankara University, 06100 Tandogan, Ankara, Turkey; (B)Istanbul Bilgi University, 34060 Eyup, Istanbul, Turkey; (C)Uludag University, 16059 Bursa, Turkey; (D)Near East University, Nicosia, North Cyprus, Mersin 10, Turkey
- ⁴⁶ University of Chinese Academy of Sciences, Beijing 100049, People's Republic of China
- ⁴⁷ University of Hawaii, Honolulu, Hawaii 96822, USA
- ⁴⁸ University of Jinan, Jinan 250022, People's Republic of China
- ⁴⁹ University of Minnesota, Minneapolis, Minnesota 55455, USA
- ⁵⁰ University of Muenster, Wilhelm-Klemm-Str. 9, 48149 Muenster, Germany
- ⁵¹ University of Science and Technology Liaoning, Anshan 114051, People's Republic of China
- ⁵² University of Science and Technology of China, Hefei 230026, People's Republic of China
- ⁵³ University of South China, Hengyang 421001, People's Republic of China
- ⁵⁴ University of the Punjab, Lahore-54590, Pakistan
- ⁵⁵ (A)University of Turin, I-10125, Turin, Italy; (B)University of Eastern Piedmont, I-15121, Alessandria, Italy; (C)INFN,

I-10125, Turin, Italy

⁵⁶ Uppsala University, Box 516, SE-75120 Uppsala, Sweden

⁵⁷ Wuhan University, Wuhan 430072, People's Republic of China

⁵⁸ Xinyang Normal University, Xinyang 464000, People's Republic of China

⁵⁹ Zhejiang University, Hangzhou 310027, People's Republic of China

⁶⁰ Zhengzhou University, Zhengzhou 450001, People's Republic of China

^a Also at Bogazici University, 34342 Istanbul, Turkey

^b Also at the Moscow Institute of Physics and Technology, Moscow 141700, Russia

^c Also at the Functional Electronics Laboratory, Tomsk State University, Tomsk, 634050, Russia

^d Also at the Novosibirsk State University, Novosibirsk, 630090, Russia

^e Also at the NRC "Kurchatov Institute", PNPI, 188300, Gatchina, Russia

^f Also at Istanbul Arel University, 34295 Istanbul, Turkey

^g Also at Goethe University Frankfurt, 60323 Frankfurt am Main, Germany

^h Also at Key Laboratory for Particle Physics, Astrophysics and Cosmology, Ministry of Education; Shanghai Key Laboratory for Particle Physics and Cosmology; Institute of Nuclear and Particle Physics, Shanghai 200240, People's Republic of China

ⁱ Government College Women University, Sialkot - 51310, Punjab, Pakistan.

^j Currently at: Center for Underground Physics, Institute for Basic Science, Daejeon 34126, Korea

Abstract

We report the first measurements of absolute branching fractions for the W -exchange-only processes $\Lambda_c^+ \rightarrow \Xi^0 K^+$ and $\Lambda_c^+ \rightarrow \Xi(1530)^0 K^+$ with the double-tag technique, by analyzing an e^+e^- collision data sample, that corresponds to an integrated luminosity of 567 pb^{-1} collected at a center-of-mass energy of 4.6 GeV by the BESIII detector. The branching fractions are measured to be $\mathcal{B}(\Lambda_c^+ \rightarrow \Xi^0 K^+) = (5.90 \pm 0.86 \pm 0.39) \times 10^{-3}$ and $\mathcal{B}(\Lambda_c^+ \rightarrow \Xi(1530)^0 K^+) = (5.02 \pm 0.99 \pm 0.31) \times 10^{-3}$, where the first uncertainties are statistical and the second systematic. Our results are more precise than the previous relative measurements.

Keywords: Λ_c^+ , W exchange, absolute branching fraction, BESIII

1. Introduction

Weak decays of charmed baryon provide useful information for understanding the interplay of weak and strong interactions, complementary to the information obtained from charmed mesons. The lightest charmed baryon Λ_c^+ is the cornerstone of the whole charmed baryon spectroscopy, and the measurement of the properties of Λ_c^+ provides essential input for studying heavier charmed baryons, such as singly and doubly charmed baryons [1, 2] and b -baryons [3]. However, theory development in describing the Λ_c^+ has been slow [4, 5, 6, 7, 8, 9, 10, 11], mostly due to limited understanding of the nontrivial non-factorizable effects involved, especially the W -exchange process. This is very different from the cases of the $D_{(s)}$ meson decays, where the W -exchange amplitude is suppressed

by color and helicity symmetries. Therefore, clean experimental measurements of the W -exchange-only process in Λ_c^+ decays play an important role in the identification of the non-factorizable contribution in different theoretical calculations [12].

The Cabibbo-favored decays $\Lambda_c^+ \rightarrow \Xi^0 K^+$ and $\Xi(1530)^0 K^+$ proceed only through the W -exchange process, as depicted in Fig. 1. These two modes are typical Λ_c^+ decays to the baryon octet and decuplet states, respectively. In these two decay modes, large cancellation between different matrix elements occur in both S - and P -wave decays, making theoretical predictions very difficult [13]. Several model predictions of the branching fractions (\mathcal{B}) for $\Lambda_c^+ \rightarrow \Xi^{(*)0} K^+$ (here and in the following, Ξ^{*0} is used to denote the $\Xi(1530)^0$) are listed in Table 1. They show large variations from each other; the predicted $\mathcal{B}(\Lambda_c^+ \rightarrow \Xi^0 K^+)$

fall in the range of $[1.0, 3.6] \times 10^{-3}$ [4, 6, 10, 14, 15], while the calculations for $\mathcal{B}(\Lambda_c^+ \rightarrow \Xi^{*0} K^+)$ give three distinct results with one-order-of-magnitude difference [4, 16, 17]. In experiment, these two modes were studied by the CLEO [18] and ARGUS [19] collaborations more than 20 years ago. Both collaborations directly measured the relative decay rates compared to $\mathcal{B}(\Lambda_c^+ \rightarrow p K^- \pi^+)$, as given in Table 1. Correcting for the branching fraction of the reference channel, $\mathcal{B}(\Lambda_c^+ \rightarrow p K^- \pi^+)$ [21, 22, 23], the average results read $\mathcal{B}(\Lambda_c^+ \rightarrow \Xi^0 K^+) = (5.0 \pm 1.2) \times 10^{-3}$ [24] and $\mathcal{B}(\Lambda_c^+ \rightarrow \Xi^{*0} K^+) = (4.0 \pm 1.0) \times 10^{-3}$ [24, 20]. Apart from the poor precision of the two \mathcal{B} 's, the experimental result for $\mathcal{B}(\Lambda_c^+ \rightarrow \Xi^0 K^+)$ exceeds the upper end of the predictions by almost 2σ . Hence, an absolute and more precise determination of these \mathcal{B} 's is an important input for the modelisation of the hadronic decays of charmed baryons.

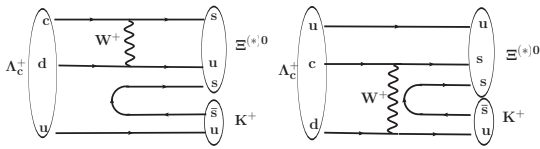


Figure 1: Feynman diagrams of $\Lambda_c^+ \rightarrow \Xi^{(*)0} K^+$.

Table 1: Comparison of previous experimental measurements and theoretical predictions for $\mathcal{B}(\Lambda_c^+ \rightarrow \Xi^{(*)0} K^+)$.

Decay	Measured $\frac{\mathcal{B}(\Lambda_c^+ \rightarrow \Xi^{(*)0} K^+)}{\mathcal{B}(\Lambda_c^+ \rightarrow p K^- \pi^+)}$	Measured $\mathcal{B}(\Lambda_c^+ \rightarrow \Xi^{(*)0} K^+)$	Predicted $\mathcal{B}(\Lambda_c^+ \rightarrow \Xi^{(*)0} K^+)$
$\Xi^0 K^+$	$(7.8 \pm 1.8)\%$ [18]	$(5.0 \pm 1.2) \times 10^{-3}$ [24]	2.6×10^{-3} [4] 3.6×10^{-3} [6] 3.1×10^{-3} [10] 1.0×10^{-3} [14] 1.3×10^{-3} [15]
$\Xi^{*0} K^+$	$(5.3 \pm 1.9)\%$ [18] $(9.3 \pm 3.2)\%$ [19, 20]	$(4.0 \pm 1.0) \times 10^{-3}$ [24, 20]	5.0×10^{-3} [4] 0.8×10^{-3} [16] 0.6×10^{-3} [17]

In this Letter, we present a study of the W -exchange-only decays $\Lambda_c^+ \rightarrow \Xi^0 K^+$ and $\Xi(1530)^0 K^+$, based on a data sample corresponding to an integrated luminosity of 567 pb^{-1} [25] collected with the BESIII detector [26] at the center-of-mass energy of $\sqrt{s} = 4.6 \text{ GeV}$. Throughout the text, charge-conjugated modes are implicitly assumed, unless otherwise stated. At this energy, Λ_c^+ is always produced in a pair accompanied by a $\bar{\Lambda}_c^-$, and the remaining phase space does not allow any additional hadrons, hence a double-tag technique [27] can be employed. This technique does not require a measurement of the luminosity and knowledge of the production cross section, thus providing a model-

independent measurement of $\mathcal{B}(\Lambda_c^+ \rightarrow \Xi^{(*)0} K^+)$. First, we select a ‘single-tag’ (ST) sample of $\bar{\Lambda}_c^-$ candidates by reconstructing the $\bar{\Lambda}_c^-$ exclusively in one of 12 hadronic decays, as described later. Then, we search for $\Lambda_c^+ \rightarrow \Xi^{(*)0} K^+$ candidates in the system recoiling against the ST side; the collection of selected candidates is referred to as the double-tag (DT) sample. In this analysis, we only detect one K^+ in the DT side and deduce the presence of a $\Xi^{(*)0}$ in the final state from four-momentum conservation. The absolute \mathcal{B} of $\Lambda_c^+ \rightarrow \Xi^{(*)0} K^+$ is then determined from the efficiency-corrected ratio of DT yields to ST yields.

2. BESIII Detector and Monte Carlo Simulation

The BESIII detector is a cylindrically symmetric detector with 93% coverage of the full solid angle around the e^+e^- interaction point (IP). The components of the apparatus are a helium-based main drift chamber (MDC), a plastic scintillator time-of-flight (TOF) system, a 6240-cell CsI(Tl) crystal electromagnetic calorimeter (EMC), a superconducting solenoid providing 1.0 T magnetic field aligned with the beam axis, and a muon counter with resistive plate chambers as the active element. The momentum resolution for charged tracks in the MDC is 0.5% at a transverse momentum of 1 GeV/c. The photon energy resolution for 1 GeV/c photos in the EMC is 2.5% in the barrel region and 5.0% in the end-cap region. The combined information of the ionization energy deposited in the MDC and the flight time measured by the TOF is used to perform particle identification (PID) for charged tracks. More details about the design and performance of the BESIII detector are given in Ref. [26].

We use high-statistics Monte Carlo (MC) simulation samples of e^+e^- annihilations to understand backgrounds and to estimate detection efficiencies. The e^+e^- annihilation is simulated by the KKMC generator [28], taking into account the beam energy spread and effects of initial-state radiation (ISR). The response of the detector to the final-state particles is simulated using GEANT4 [29]. Inclusive MC samples, consisting of generic $\Lambda_c^+ \bar{\Lambda}_c^-$ events, $D_{(s)}^* \bar{D}_{(s)}^* + X$ production [30], ISR return to the charmonium(-like) ψ states at lower masses, and continuum processes $e^+e^- \rightarrow q\bar{q}$ ($q = u, d, s$) are generated to study the backgrounds and to estimate the ST detection efficiencies. Exclusive DT signal MC events, where the $\bar{\Lambda}_c^-$ decays into the studied ST modes and the Λ_c^+ decays into $\Xi^0 K^+$ or $\Xi^{*0} K^+$ (with Ξ^0 and Ξ^{*0} decaying generically to all known channels), are used to determine the DT detection efficiencies. All assumed simulated decay rates are taken

from in Ref. [24], and the decays are generated using EVTGEN [31].

For the MC production of $e^+e^- \rightarrow \Lambda_c^+ \bar{\Lambda}_c^-$ events, the observed cross sections are taken into account, and phase space generated $\bar{\Lambda}_c^-$ decays are re-weighted according to the observed features in data. For the decays of $\Lambda_c^+ \rightarrow \Xi^{(*)0} K^+$, the angular distributions of K^+ are generated following $1 + \alpha_{\Xi^{(*)}K} \cos^2 \theta_K$, where θ_K is the polar angle of the K^+ in the rest system of the Λ_c^+ . The parameters $\alpha_{\Xi^{(*)}K}$ in these two decays are determined from our measurement, as discussed later.

3. Analysis

The ST $\bar{\Lambda}_c^-$ baryon candidates are reconstructed using 12 hadronic decay modes: $\bar{\Lambda}_c^- \rightarrow \bar{p} K_S^0$, $\bar{p} K^+ \pi^-$, $\bar{p} K_S^0 \pi^0$, $\bar{p} K_S^0 \pi^- \pi^+$, $\bar{p} K^+ \pi^- \pi^0$, $\bar{p} \pi^- \pi^+$, $\bar{\Lambda} \pi^-$, $\bar{\Lambda} \pi^- \pi^0$, $\bar{\Lambda} \pi^- \pi^+ \pi^-$, $\bar{\Sigma}^0 \pi^-$, $\bar{\Sigma}^- \pi^0$, and $\bar{\Sigma}^- \pi^- \pi^+$. Here, the intermediate particles K_S^0 , $\bar{\Lambda}$, $\bar{\Sigma}^0$, $\bar{\Sigma}^-$ and π^0 are reconstructed through their decays $K_S^0 \rightarrow \pi^+ \pi^-$, $\bar{\Lambda} \rightarrow \bar{p} \pi^+$, $\bar{\Sigma}^0 \rightarrow \gamma \bar{\Lambda}$, $\bar{\Sigma}^- \rightarrow \bar{p} \pi^0$, and $\pi^0 \rightarrow \gamma \gamma$, respectively.

Charged tracks are required to satisfy $|\cos \theta| < 0.93$, where θ is the polar angle with respect to the positron beam direction. Their distances of closest approaches to the IP are required to be less than 10 cm and 1 cm along and in the plane perpendicular to the electron beam axis, respectively. Tracks are identified as protons if their PID likelihood (\mathcal{L}) satisfies $\mathcal{L}(p) > \mathcal{L}(K)$ and $\mathcal{L}(p) > \mathcal{L}(\pi)$, while charged kaons and pions are selected using $\mathcal{L}(K) > \mathcal{L}(\pi)$ and $\mathcal{L}(\pi) > \mathcal{L}(K)$, respectively. More information related to PID in BESIII can be found elsewhere [11].

Clusters in the EMC not associated with any charged track are identified as photon candidates if they satisfy the following requirements: the deposited energy is required to be larger than 25 MeV in the barrel region ($|\cos \theta| < 0.8$) or 50 MeV in the end-cap region ($0.86 < |\cos \theta| < 0.92$). To suppress background from electronic noise and showers unrelated to the event, the shower time measured by the EMC relative to the event start time is required to be between 0 and 700 ns. The π^0 candidates are reconstructed from photon pairs that have an invariant mass satisfying $115 < M(\gamma\gamma) < 150 \text{ MeV}/c^2$. To improve the momentum resolution, a kinematic fit constraining the invariant mass to the π^0 nominal mass [24] is applied to the photon pairs and the resulting energy and momentum of the π^0 are used for further analysis.

Candidates for K_S^0 and $\bar{\Lambda}$ are formed by combining two oppositely charged tracks of $\pi^+ \pi^-$ and $\bar{p} \pi^+$, respectively. For these two tracks, their distances of

closest approaches to the IP must be within ± 20 cm along the electron beam direction. No distance constraints in the transverse plane are required. The two daughter tracks are constrained to originate from a common decay vertex by requiring the χ^2 of the vertex fit to be less than 100. Furthermore, the decay vertex is required to be separated from the IP by a distance greater than twice the fitted vertex resolution. In this procedure, as the combinational backgrounds have been highly suppressed, the charged pions are not subjected to the PID requirement described above, to have the optimal signal significance. The vertex fitted momenta of the daughter particles are used in the further analysis. We impose the requirements $487 < M(\pi^+ \pi^-) < 511 \text{ MeV}/c^2$ and $1111 < M(\bar{p} \pi^+) < 1121 \text{ MeV}/c^2$ for K_S^0 and $\bar{\Lambda}$ candidates. The $\bar{\Sigma}^0$ and $\bar{\Sigma}^-$ candidates are reconstructed from any combinations of $\bar{\Lambda} \gamma$ and $\bar{p} \pi^0$ with requirement $1179 < M(\bar{\Lambda} \gamma) < 1203 \text{ MeV}/c^2$ and $1176 < M(\bar{p} \pi^0) < 1200 \text{ MeV}/c^2$, respectively. The above requirements on the invariant masses correspond to approximately ± 3 standard deviations around the nominal masses [24]. For the decay modes $\bar{p} K_S^0 \pi^0$, $\bar{p} K_S^0 \pi^- \pi^+$, $\bar{p} \pi^- \pi^+$ and $\bar{\Sigma}^- \pi^- \pi^+$, possible backgrounds including $\bar{\Lambda} \rightarrow \bar{p} \pi^+$ in the final state are rejected by requiring $M(\bar{p} \pi^+)$ to be out of the range $(1110, 1120) \text{ MeV}/c^2$. In addition, $\bar{p} K_S^0 \pi^0$ candidates satisfying $1170 < M(\bar{p} \pi^0) < 1200 \text{ MeV}/c^2$ are excluded to suppress the backgrounds with a $\bar{\Sigma}^-$ in the final state. To remove K_S^0 candidates in the modes $\bar{p} \pi^- \pi^+$, $\bar{\Lambda} \pi^- \pi^+ \pi^-$, $\bar{\Sigma}^- \pi^0$ and $\bar{\Sigma}^- \pi^- \pi^+$, the mass of any $\pi^+ \pi^-$ and $\pi^0 \pi^0$ pair is not allowed to fall in the range $(480, 520) \text{ MeV}/c^2$.

The ST $\bar{\Lambda}_c^-$ yields are identified using the beam-constrained mass $M_{\text{BC}} \equiv \sqrt{E_{\text{beam}}^2/c^4 - p^2/c^2}$, where E_{beam} is the average value of the e^+ and e^- beam energies and p is the measured $\bar{\Lambda}_c^-$ momentum in the center-of-mass system of the e^+e^- collision. To improve the signal purity, the energy difference $\Delta E \equiv E - E_{\text{beam}}$ for the $\bar{\Lambda}_c^-$ candidate is required to fulfill a mode-dependent ΔE requirement shown in Table 2, corresponding to approximately three times the resolutions. Here, E is the total reconstructed energy of the $\bar{\Lambda}_c^-$ candidate. For each ST decay mode, if more than one candidate satisfies the above requirements, we select the one with minimal $|\Delta E|$. Figure 2 shows the M_{BC} distributions for the ST samples, where evident $\bar{\Lambda}_c^-$ signals peak at the nominal $\bar{\Lambda}_c^-$ mass [24]. We follow the procedure described in Ref. [22] to determine the ST yields for a given tag mode i [N_i^{ST}] in the signal region $2282 < M_{\text{BC}} < 2291 \text{ MeV}/c^2$ and the corresponding detection efficiencies [$\varepsilon_i^{\text{ST}}$], as summarized in Table 2. In the procedure of extracting detection effi-

ciencies, the M_{BC} resolutions in MC samples are corrected to agree with those in data. Besides, MC simulations show that peaking backgrounds in some ST modes are observed with a yield of 1% or less that of the signal.

Table 2: Requirements on ΔE , ST yields N_i^{ST} and detection efficiencies $\varepsilon_i^{\text{ST}}$, and DT efficiencies of $\varepsilon_{i,\Xi K}^{\text{DT}}$ and $\varepsilon_{i,\Xi^* K}^{\text{DT}}$. The uncertainties are statistical only. The quoted efficiencies do not include any subleading \mathcal{B} .

Mode	ΔE (MeV)	N_i^{ST}	$\varepsilon_i^{\text{ST}}(\%)$	$\varepsilon_{i,\Xi K}^{\text{DT}}(\%)$	$\varepsilon_{i,\Xi^* K}^{\text{DT}}(\%)$
$\bar{p}K_S^0$	(-20, 20)	1145 \pm 34	51.6	41.2	42.6
$\bar{p}K^+\pi^-$	(-20, 20)	5722 \pm 80	45.2	37.3	39.1
$\bar{p}K_S^0\pi^0$	(-30, 20)	478 \pm 28	17.2	15.1	15.2
$\bar{p}K_S^0\pi^-\pi^+$	(-20, 20)	431 \pm 25	18.6	15.4	15.2
$\bar{p}K^+\pi^-\pi^0$	(-30, 20)	1407 \pm 51	14.7	13.4	12.7
$\bar{p}\pi^-\pi^+$	(-20, 20)	474 \pm 41	55.4	43.3	45.1
$\bar{\Lambda}\pi^-$	(-20, 20)	648 \pm 25	38.7	30.9	31.4
$\bar{\Lambda}\pi^-\pi^0$	(-30, 20)	1282 \pm 43	13.0	10.9	11.2
$\bar{\Lambda}\pi^-\pi^+\pi^-$	(-20, 20)	540 \pm 27	10.6	9.0	8.8
$\bar{\Sigma}^0\pi^-$	(-20, 20)	427 \pm 23	24.1	20.6	20.6
$\bar{\Sigma}^-\pi^0$	(-50, 30)	258 \pm 20	19.6	17.3	17.4
$\bar{\Sigma}^-\pi^-\pi^+$	(-30, 20)	1005 \pm 42	20.1	17.2	18.1

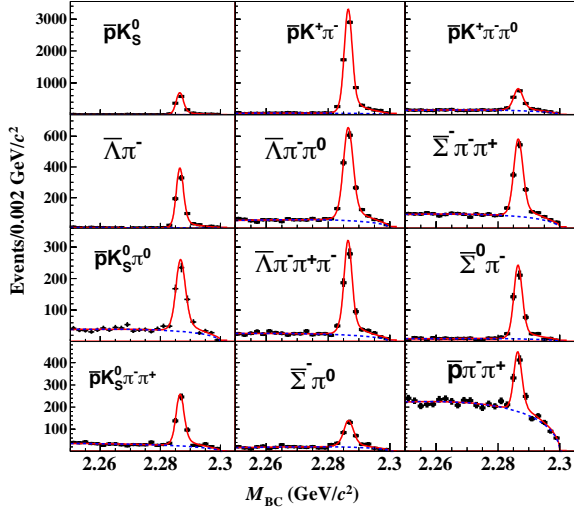


Figure 2: Fits to the M_{BC} distributions in data for the different ST modes. Points with error bars are data, solid lines are the sum of the fit functions, and dashed lines are the background shapes.

Candidates of $\Lambda_c^+ \rightarrow \Xi^{(*)0} K^+$ decays are reconstructed from the remaining tracks recoiling against the ST $\bar{\Lambda}_c^-$. A kaon with opposite charge to the tagged $\bar{\Lambda}_c^-$ is selected with the same selection criteria as described above. No multiple DT candidates in an event are observed. The kinematic variable

$$M_{\text{miss}} \equiv \sqrt{E_{\text{miss}}^2/c^4 - |\vec{p}_{\text{miss}}|^2/c^2}, \quad (1)$$

is used to infer the undetected Ξ^0 and Ξ^{*0} , where E_{miss} and \vec{p}_{miss} are the missing energy and momentum carried away by the undetected Ξ^0 or Ξ^{*0} . The E_{miss} and \vec{p}_{miss} are calculated by $E_{\text{miss}} \equiv E_{\text{beam}} - E_{K^+}$ and $\vec{p}_{\text{miss}} \equiv \vec{p}_{\Lambda_c^+} - \vec{p}_{K^+}$, where $E_{K^+}(\vec{p}_{K^+})$ is the energy (momentum) of the K^+ in the e^+e^- center-of-mass system. The momentum of the Λ_c^+ baryon $\vec{p}_{\Lambda_c^+}$ is calculated by $\vec{p}_{\Lambda_c^+} \equiv -\hat{p}_{\text{tag}} \sqrt{E_{\text{beam}}^2/c^2 - m_{\Lambda_c^+}^2/c^2}$, where \hat{p}_{tag} is the momentum direction of the ST $\bar{\Lambda}_c^-$ and $m_{\Lambda_c^+}$ is the nominal mass of the Λ_c^+ [24]. For the signal $\Lambda_c^+ \rightarrow \Xi^{(*)0} K^+$ decay, M_{miss} is expected to peak at the the nominal masses of the Ξ^0 and Ξ^{*0} , *i.e.* at 1314.9 MeV/ c^2 and 1531.8 MeV/ c^2 , respectively [24].

We combine the DT candidates over the 12 ST modes and plot the resulting M_{miss} distribution in Fig. 3. An unbinned maximum likelihood fit is performed to determine DT signal yields. The $\Lambda_c^+ \rightarrow \Xi^{(*)0} K^+$ signal shape is obtained from the MC-derived signal shape convolved with a Gaussian function common to both signal channels whose parameters are left free in the fit. The background shape is described by a quadratic function, which is validated by the candidate events in the ST M_{BC} sideband region of data and the MC-simulated background samples. Figure 3 shows the fitted curves to the M_{miss} distribution. We obtain the DT signal yields of $\Xi^0 K^+$ and $\Xi^{*0} K^+$ to be $N_{\Xi K}^{\text{DT}} = 68.2 \pm 9.9$ and $N_{\Xi^* K}^{\text{DT}} = 59.5 \pm 11.7$, respectively, where the uncertainties are statistical only. The statistical significances for the signal are evaluated by the changes in the likelihood between the nominal fit and a fit with the signal yield set to zero; they are 10.3σ for $\Xi^0 K^+$ and 6.4σ for $\Xi^{*0} K^+$.

The absolute \mathcal{B} for $\Lambda_c^+ \rightarrow \Xi^0 K^+$ and $\Lambda_c^+ \rightarrow \Xi^{*0} K^+$ are obtained by the following formula

$$\mathcal{B}(\Lambda_c^+ \rightarrow \Xi^{(*)0} K^+) = \frac{N_{\Xi^{(*)} K}^{\text{DT}}}{\sum_i \frac{N_i^{\text{ST}}}{\varepsilon_i^{\text{ST}}} \varepsilon_{i,\Xi^{(*)} K}^{\text{DT}}}. \quad (2)$$

The DT efficiencies $\varepsilon_{i,\Xi^{(*)} K}^{\text{DT}}$ are evaluated based on the yields of the DT signal MC samples in the M_{miss} signal window (1.10, 1.65) GeV/ c^2 , as summarized in Table 2. Using Eq. (2), we obtain $\mathcal{B}(\Lambda_c^+ \rightarrow \Xi^0 K^+) = (5.90 \pm 0.86 \pm 0.39) \times 10^{-3}$ and $\mathcal{B}(\Lambda_c^+ \rightarrow \Xi^{*0} K^+) = (5.02 \pm 0.99 \pm 0.31) \times 10^{-3}$, where the first uncertainties are statistical and the second systematic as described below.

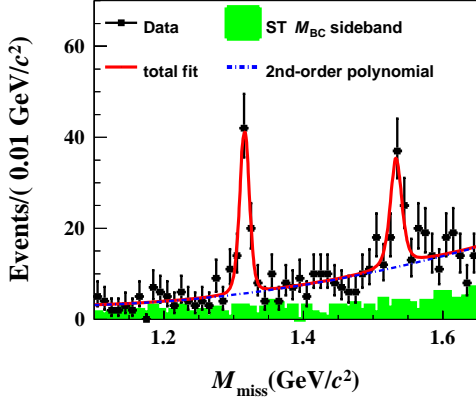


Figure 3: Fit to the M_{miss} distribution of the DT candidates. Points with error bars are data, the solid line is the sum of fit functions, the dash-dotted line is the quadratic function for background and the shaded histogram shows normalized data from the ST M_{BC} sideband region, defined as $2.250 < M_{\text{BC}} < 2.265 \text{ GeV}/c^2$.

As the DT technique is adopted, the systematic uncertainties originating from reconstructing the ST side cancel. The systematic uncertainties in the $\mathcal{B}(\Lambda_c^+ \rightarrow \Xi^0 K^+)$ and $\mathcal{B}(\Lambda_c^+ \rightarrow \Xi^{*0} K^+)$ measurements mainly arise from possible differences between the data and MC simulation of signal processes, K^+ tracking, K^+ PID, the fit to the M_{miss} distribution, ST peaking backgrounds, and the M_{BC} ST distributions. The detailed estimation of the different systematic uncertainties are given below.

The signal processes $\Lambda_c^+ \rightarrow \Xi^{(*)0} K^+$ are simulated by taking into account the angular dependences $1 + \alpha_{\Xi^{(*)}K} \cos^2 \theta_K$. We obtain the parameters $\alpha_{\Xi^0 K} = 0.77 \pm 0.78$ and $\alpha_{\Xi^{*0} K} = -1.00 \pm 0.34$ from fits to data, where the statistical uncertainties are dominant. The uncertainties from signal MC modeling are determined to be 3.2% and 3.9% for $\Lambda_c^+ \rightarrow \Xi^0 K^+$ and $\Lambda_c^+ \rightarrow \Xi^{*0} K^+$ respectively, by changing the parameter $\alpha_{\Xi^{(*)}K}$ within the uncertainties.

The uncertainties associated with K^+ tracking and PID are estimated to be 1.0% each by studying a set of control samples of $e^+e^- \rightarrow K^+K^-\pi^+\pi^-$ events selected from data taken at energies above $\sqrt{s} = 4.0 \text{ GeV}$. The uncertainties due to the fit procedure are estimated to be 5.2% and 3.7% for $\Lambda_c^+ \rightarrow \Xi^0 K^+$ and $\Lambda_c^+ \rightarrow \Xi^{*0} K^+$, respectively, by varying the fit range and background shape. In order to estimate the overall uncertainties due to the ST peaking backgrounds, we estimate the ratio of peaking background contributing to the total ST yields for each ST mode, and then reweight these ratios by the ST yields N_i^{ST} obtained in data. We eval-

uate the resultant systematic uncertainties to be 0.8% for both $\Lambda_c^+ \rightarrow \Xi^0 K^+$ and $\Lambda_c^+ \rightarrow \Xi^{*0} K^+$. A possible bias to the efficiency ratio of the DT and ST selections due to the M_{BC} resolution correction is explored by removing the corresponding correction in MC samples. The efficiency ratios are re-calculated and the deviations of 2.2% and 2.4% to the nominal results are taken as the systematic uncertainties for $\Lambda_c^+ \rightarrow \Xi^0 K^+$ and $\Lambda_c^+ \rightarrow \Xi^{*0} K^+$, respectively. All these systematic uncertainties are summarized in Table 3, and the total systematic uncertainties are evaluated to be 6.7% and 6.1% for $\Lambda_c^+ \rightarrow \Xi^0 K^+$ and $\Lambda_c^+ \rightarrow \Xi^{*0} K^+$, respectively, by summing up all the contributions in quadrature.

Table 3: Sources of systematic uncertainties and the corresponding relative values.

Source	$\Xi^0 K^+$ (%)	$\Xi^{*0} K^+$ (%)
MC model	3.2	3.9
Tracking	1.0	1.0
PID	1.0	1.0
Fitting	5.2	3.7
ST peaking background	0.8	0.8
M_{BC} requirement	2.2	2.4
Total	6.7	6.1

4. Summary

To summarize, the absolute branching fractions of two W -exchange-only processes $\Lambda_c^+ \rightarrow \Xi^0 K^+$ and $\Lambda_c^+ \rightarrow \Xi(1530)^0 K^+$ are measured by employing a double-tag technique, based on a sample of threshold produced data at $\sqrt{s} = 4.6 \text{ GeV}$ collected with BESIII detector. The results are $\mathcal{B}(\Lambda_c^+ \rightarrow \Xi^0 K^+) = (5.90 \pm 0.86 \pm 0.39) \times 10^{-3}$ and $\mathcal{B}(\Lambda_c^+ \rightarrow \Xi(1530)^0 K^+) = (5.02 \pm 0.99 \pm 0.31) \times 10^{-3}$, where the first uncertainties are statistical and the second systematic. These are the first absolute measurements of the branching fractions for the $\Lambda_c^+ \rightarrow \Xi^0 K^+$ and $\Lambda_c^+ \rightarrow \Xi(1530)^0 K^+$ decays. The results are consistent with the previous measurements [18, 19], but have improved precision. For the $\Xi^0 K^+$ mode, the combined \mathcal{B} gives $(5.56 \pm 0.74) \times 10^{-3}$, which shows more significant deviations from predicted values in Table 1 by at least 2.6σ . The measured $\mathcal{B}(\Lambda_c^+ \rightarrow \Xi(1530)^0 K^+)$ favors the calculation in Ref. [4], while $\mathcal{B}(\Lambda_c^+ \rightarrow \Xi^0 K^+)$ in Ref. [4] has 4σ discrepancy from experimental result. This indicates that our results are essential to calibrate the W -exchange diagram amplitudes in these theoretical approaches.

5. Acknowledgments

The BESIII collaboration thanks the staff of BEPCII and the IHEP computing center for their strong support. This work is supported in part by National Key Basic Research Program of China under Contract No. 2015CB856700; National Natural Science Foundation of China (NSFC) under Contracts Nos. 11235011, 11335008, 11425524, 11625523, 11635010; the Chinese Academy of Sciences (CAS) Large-Scale Scientific Facility Program; the CAS Center for Excellence in Particle Physics (CCEPP); Joint Large-Scale Scientific Facility Funds of the NSFC and CAS under Contracts Nos. U1332201, U1532257, U1532258; CAS Key Research Program of Frontier Sciences under Contracts Nos. QYZDJ-SSW-SLH003, QYZDJ-SSW-SLH040; CAS under Contracts Nos. KJCX2-YW-N29, KJCX2-YW-N45, QYZDJ-SSW-SLH003; 100 Talents Program of CAS; National 1000 Talents Program of China; INPAC and Shanghai Key Laboratory for Particle Physics and Cosmology; German Research Foundation DFG under Contracts Nos. Collaborative Research Center CRC 1044, FOR 2359; Istituto Nazionale di Fisica Nucleare, Italy; Koninklijke Nederlandse Akademie van Wetenschappen (KNAW) under Contract No. 530-4CDP03; Ministry of Development of Turkey under Contract No. DPT2006K-120470; National Science and Technology fund; The Swedish Research Council; U. S. Department of Energy under Contracts Nos. DE-FG02-05ER41374, DE-SC-0010118, DE-SC-0010504, DE-SC-0012069; University of Groningen (RuG) and the Helmholtzzentrum fuer Schwerionenforschung GmbH (GSI), Darmstadt; WCU Program of National Research Foundation of Korea under Contract No. R32-2008-000-10155-0; China Postdoctoral Science Foundation; This paper is also supported by Beijing municipal government under Contract No. CIT&TCD201704047.

References

- [1] C. Q. Geng, Y. K. Hsiao, C. W. Liu and T. H. Tsai, *JHEP* **1711**, 147 (2017).
- [2] F. S. Yu, H. Y. Jiang, R. H. Li, C. D. Lü, W. Wang and Z. X. Zhao, arXiv:1703.09086 [hep-ph].
- [3] J. L. Rosner, *Phys. Rev. D* **86**, 014017 (2012).
- [4] J. G. Körner and M. Krämer, *Z. Phys. C* **55**, 659 (1992).
- [5] T. Uppal, R. C. Verma and M. P. Khanna, *Phys. Rev. D* **49**, 3417 (1994).
- [6] P. Zenczykowski, *Phys. Rev. D* **50**, 402 (1994).
- [7] L. L. Chau, H. Y. Cheng and B. Tseng, *Phys. Rev. D* **54**, 2132 (1996).
- [8] K. K. Sharma and R. C. Verma, *Phys. Rev. D* **55**, 7067 (1997).
- [9] Y. Kohara, *Nuovo Cim. A* **111**, 67 (1998).
- [10] M. A. Ivanov, J. G. Körner, V. E. Lyubovitskij and A. G. Rusetsky, *Phys. Rev. D* **57**, 5632 (1998).
- [11] D. M. Asner *et al.*, *Int. J. Mod. Phys. A* **24**, S1 (2009)
- [12] H. Y. Cheng, *Front. Phys.* **10**, 101406 (2015).
- [13] H. Y. Cheng and B. Tseng, *Phys. Rev. D* **48**, 4188 (1993)
- [14] Q. P. Xu and A. N. Kamal, *Phys. Rev. D* **46**, 270 (1992).
- [15] K. K. Sharma and R. C. Verma, *Eur. Phys. J. C* **7**, 217 (1999).
- [16] Q. P. Xu and A. N. Kamal, *Phys. Rev. D* **46**, 3836 (1992).
- [17] Fayyazuddin and Riazuddin, *Phys. Rev. D* **55**, 255 (1997) Erratum: [*Phys. Rev. D* **56**, 531 (1997)].
- [18] P. Avery *et al.* [CLEO Collaboration], *Phys. Rev. Lett.* **71**, 2391 (1993).
- [19] H. Albrecht *et al.* [ARGUS Collaboration], *Phys. Lett. B* **342**, 397 (1995).
- [20] The branching fraction of $\Xi(1530)^0 \rightarrow \Xi^- \pi^+$ is assumed to be $\frac{2}{3}$ and it is used to correct the ARGUS measurement in Ref. [19].
- [21] A. Zupanc *et al.* [Belle Collaboration], *Phys. Rev. Lett.* **113**, 042002 (2014).
- [22] M. Ablikim *et al.* [BESIII Collaboration], *Phys. Rev. Lett.* **116**, 052001 (2016).
- [23] Y. Amhis *et al.*, *Eur. Phys. J. C* **77**, 895 (2017).
- [24] C. Patrignani *et al.* [Particle Data Group], *Chin. Phys. C* **40**, 100001 (2016) and 2017 update.
- [25] M. Ablikim *et al.* [BESIII Collaboration], *Chin. Phys. C* **39**, 093001 (2015).
- [26] M. Ablikim *et al.* [BESIII Collaboration], *Nucl. Instrum. Meth. A* **614**, 345 (2010).
- [27] R. M. Baltrusaitis *et al.* [MARK-III Collaboration], *Phys. Rev. Lett.* **56**, 2140 (1986); J. Adler *et al.* [MARK-III Collaboration], *Phys. Rev. Lett.* **60**, 89 (1988).
- [28] S. Jadach *et al.*, *Phys. Rev. D* **63**, 113009 (2001).
- [29] S. Agostinelli *et al.* [GEANT Collaboration], *Nucl. Instrum. Meth. A* **506**, 250 (2003); J. Allison *et al.*, *IEEE Trans. Nucl. Sci.* **53**, 270 (2006).
- [30] N. Brambilla *et al.*, *Eur. Phys. J. C* **71**, 1534 (2011).
- [31] D. J. Lange, *Nucl. Instrum. Meth. A* **462**, 152 (2001); R. G. Ping, *Chin. Phys. C* **32**, 599 (2008).